



**HAL**  
open science

## Surface soil moisture estimation over the AMMA Sahelian site in Mali using ENVISAT/ASAR data

Frédéric Baup, Éric Mougin, Patricia de Rosnay, Franck Timouk, I. Chênerie

► **To cite this version:**

Frédéric Baup, Éric Mougin, Patricia de Rosnay, Franck Timouk, I. Chênerie. Surface soil moisture estimation over the AMMA Sahelian site in Mali using ENVISAT/ASAR data. *Remote Sensing of Environment*, 2007, 109 (4), pp.473-481. 10.1016/j.rse.2007.01.015 . ird-00391966

**HAL Id: ird-00391966**

**<https://ird.hal.science/ird-00391966>**

Submitted on 5 Jun 2009

**HAL** is a multi-disciplinary open access archive for the deposit and dissemination of scientific research documents, whether they are published or not. The documents may come from teaching and research institutions in France or abroad, or from public or private research centers.

L'archive ouverte pluridisciplinaire **HAL**, est destinée au dépôt et à la diffusion de documents scientifiques de niveau recherche, publiés ou non, émanant des établissements d'enseignement et de recherche français ou étrangers, des laboratoires publics ou privés.



ELSEVIER

Available online at [www.sciencedirect.com](http://www.sciencedirect.com)



Remote Sensing of Environment xx (2007) xxx–xxx

Remote Sensing  
of  
Environment

[www.elsevier.com/locate/rse](http://www.elsevier.com/locate/rse)

# Surface soil moisture estimation over the AMMA Sahelian site in Mali using ENVISAT/ASAR data

F. Baup<sup>a,b,\*</sup>, E. Mougin<sup>a</sup>, P. de Rosnay<sup>a</sup>, F. Timouk<sup>a</sup>, I. Chênerie<sup>b</sup>

<sup>a</sup> CESBIO (UPS-CNRS-CNES-IRD) 18 Avenue Edouard Belin 31401 Toulouse Cedex 9, France

<sup>b</sup> ADMM Université Paul Sabatier 118 Route de Narbonne 31062 Toulouse Cedex 9, France

Received 10 July 2006; received in revised form 29 January 2007; accepted 29 January 2007

## Abstract

This paper focuses on different methods for estimating soil moisture in a Sahelian environment by comparing ENVISAT/ASAR and ground data at the same spatial scale. The analysis is restricted to Wide Swath data in order to take advantage of their high temporal repetitivity (about 3–4 days) corresponding to a moderate spatial resolution (150 m). On the one hand, emphasis is put on the characterization of Surface Soil Moisture (SSM) at a spatial scale compatible with the derivation of the backscattering coefficients, and a transfer function is developed for up-scaling local measurements to the 1 km scale. On the other hand, three different approaches are used to normalize the angular variation of the observed backscattering coefficients. The results show a strong linear relationship between the HH normalized backscattering coefficients and SSM. The best result is obtained when restricting the ASAR data to low incidence angles and by taking into account vegetation effects using multi-angular radar data. For this case, the rms error of the SSM retrieval is 2.8%. These results highlight the capabilities of the ASAR instrument to monitor SSM in a semiarid environment.

© 2007 Published by Elsevier Inc.

**Keywords:** ENVISAT; ASAR; Wide Swath; Sahel; Soil moisture

## 1. Introduction

West Africa and more specifically the Sahelian zone has been identified by [Koster et al. \(2004\)](#) to be one among several regions of the world with the most significant feedback between soil moisture and precipitation. This hot spot “indicates where the routine monitoring of soil moisture, with both ground-based and space-based systems, will yield the greatest return in boreal summer seasonal forecasting”. Monitoring the spatial and temporal variability of soil moisture is also critical for understanding soil–vegetation–atmosphere interactions and to address the role of soil moisture on West African Monsoon dynamics ([Clark et al., 2004](#); [Monteny et al., 1997](#); [Taylor & Ellis, 2006](#); [Taylor et al., 2005](#)). Accordingly, soil moisture monitoring over the Sahel is a critical issue of the AMMA project (African Monsoon Multidisciplinary Analysis) which aims at providing a better understanding of the West African

Monsoon and its physical, chemical and biological environments ([GEWEX-news, 2006](#)).

Microwave remote sensing technology has demonstrated a quantitative ability to measure soil moisture under a variety of topographic and vegetation cover conditions. It provides spatially integrated information on soil moisture at a scale relevant for atmospheric processes and it is suitable to be extended to routine measurements from satellite systems ([Engman, 1990](#)). Several large-scale field experiments, including aircraft microwave radiometric observations, have been conducted within the framework of HAPEX, FIFE and Monsoon’90 ([Schmugge et al., 1992](#)). In semiarid regions, the relevance of aircraft L-band measurements to characterize soil moisture dynamics has been shown by [Chanzy et al. \(1997\)](#). Spaceborne systems, such as the Advanced Microwave Scanning Radiometer, AMSR-E, currently provide accurate estimates of Surface Soil Moisture (SSM) content ([Njoku et al., 2003](#)). However, only coarse spatial resolutions (> 10 km) are applicable using such methods.

Similarly, spaceborne C-band scatterometers with a high temporal sampling (4–5 days in theory) corresponding to a

\* Corresponding author. CESBIO (UPS-CNRS-CNES-IRD) 18 Avenue Edouard Belin 31401 Toulouse Cedex 9, France.

E-mail address: [frederic.baup@cesbio.cnes.fr](mailto:frederic.baup@cesbio.cnes.fr) (F. Baup).

58 spatial resolution of about 50 km have shown considerable  
 59 potential for monitoring soil moisture over semiarid areas  
 60 (Frison et al., 1998; Wagner & Scipal, 2000; Woodhouse &  
 61 Hoekman, 2000). In particular, observations made at low  
 62 incidence angles are found to be significantly related to SSM  
 63 (Frison et al., 1998; Jarlan et al., 2002, 2003; Magagi & Kerr,  
 64 1997; Stephen & Long, 2004). Compared to scatterometers,  
 65 Synthetic Aperture Radars (SAR) such as those onboard the  
 66 European Remote Sensing (ERS) and ENVISAT satellites offer  
 67 a better spatial resolution (30 m) but at the expense of a lower  
 68 frequency temporal sampling (only 35 days for ENVISAT). The  
 69 potential of both SAR and scatterometers for detecting changes  
 70 in SSM results from their high sensitivity to the variation of the  
 71 dielectric properties of the surface that are mainly linked to  
 72 changes in SSM (Satalino et al., 2002; Ulaby & Batlivala, 1976;  
 73 Ulaby et al., 1986; Zribi et al., 2003). Moreover, in semi-arid  
 74 regions and at low incidence angles, vegetation effects are  
 75 minimized or can be taken into account using relatively simple  
 76 methods (Moran et al., 2000; Tansey et al., 1999). In terms of  
 77 dominantly vertically-orientated herbaceous vegetation, the use  
 78 of the HH polarization is expected to improve the SSM estim-  
 79 ation from space due to the corresponding larger SSM  
 80 sensitivity, especially at low incidence angle (Ulaby, 1975).

81 The present study focuses on examining the relationships  
 82 between backscattering coefficient data acquired by the ASAR  
 83 instrument at HH polarization and soil moisture measurements

84 recorded in a Sahelian environment. Here, only the ASAR Wide  
 85 Swath data are used in order to take advantage of their high  
 86 temporal sampling of 3–4 days associated with a moderate  
 87 spatial resolution (150 m). The considered period is July–  
 88 December 2005, which includes the entire rainy season. The  
 89 paper is organized as follows: The study site, the associated data  
 90 and the methodology are presented in Section 2. Three simple  
 91 methods to normalize the radar data acquired at different  
 92 incidence angles are described, and the interest in using LAI  
 93 data for improving the angular normalization is explained.  
 94 Section 3 presents the results of a correlation analysis based on  
 95 the three different methods. Conclusions and Perspectives are  
 96 given in Section 4.

## 97 2. Data and methods

### 98 2.1. The study site

99 The Agoufou (15.3°N, 1.3°W) study site is located within  
 100 the AMMA meso-scale site (14.5–17.5°N, 1–2°W) in the  
 101 Gourma region in Mali (Fig. 1). The Gourma region is located  
 102 entirely within the Sahel bioclimatic zone and extends to the  
 103 South of the Niger River between Timbuctu and Gao down to  
 104 the border with Burkina-Faso. This is mainly a pastoral region  
 105 enclosed by the annual average 500 and 150 mm isohyets. The  
 106 rain distribution is strictly mono-modal with rainfall starting in

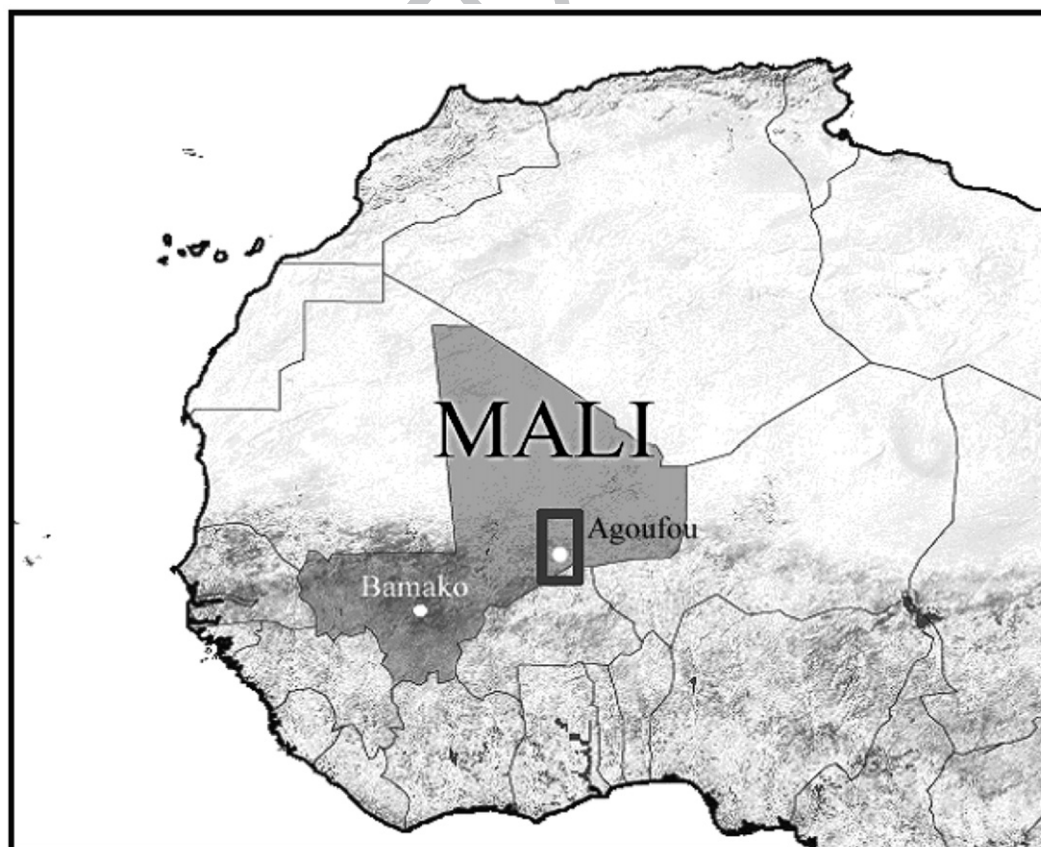


Fig. 1. The Gourma window in Mali showing the Agoufou site (●).

107 June and ending in September with a maximum in August. The  
 108 rainy season is then followed by a long dry season characterized  
 109 by the absence of green vegetation apart from some scattered  
 110 trees and shrubs. Rangeland vegetation is composed of a  
 111 herbaceous layer and a sparse woody plant population. Herb  
 112 growth is strongly influenced by the pattern and magnitude of  
 113 rainfall events and by the soil moisture regime that results from  
 114 them and from run-off influenced by topography and soil  
 115 texture. Annual herbs germinate after the first rains, in June or  
 116 July, and unless the plants wilt before maturity owing to a lack  
 117 of rainfall, the senescence coincides approximately with the end  
 118 of the rainy season.

119 The Agoufou site ( $1 \times 1 \text{ km}^2$ ) is a typical Sahelian landscape  
 120 characterized by gently undulating sand dunes (Fig. 2). The  
 121 altitude ranges between 302 and 310 meters above sea level.  
 122 The total tree and shrub cover is about 4.5%, whereas the grass  
 123 cover may vary from 0 to about 60% depending on soil moisture  
 124 availability. The soil is coarse grained or sandy (>90%).

125 For the 2005 wet season, the annual rainfall total is 408 mm  
 126 which can be considered as a relatively wet year (the long-term  
 127 average is 370 mm). Ground measurements of the vegetation  
 128 consist in an estimate of the time variation of LAI from trees and  
 129 grasses using hemispherical photographs (Weiss et al., 2004).  
 130 For the grass layer, a 1 km transect has been defined in the E–W  
 131 direction where measurements are performed every 10 m,  
 132 resulting in 100 pictures. The large quantity of data is sufficient  
 133 to capture the spatial variability of the grass layer. The computed  
 134 mean LAI is assumed to be representative at the  $1 \text{ km}^2$  scale. The  
 135 estimated resulting accuracy is  $0.23 \text{ m}^2 \text{ m}^{-2}$  (at 1 S.D.).

136 In 2005, the growth of the grass layer started early in June  
 137 and reached a maximum LAI of 1.8 by the end of August  
 138 (Fig. 3). In contrast, the LAI of trees estimated from pictures  
 139 taken of isolated individual stands remains at values lower than  
 140 0.2 throughout the year. Accordingly, trees are not considered in  
 141 this study.

## 2.2. Surface soil moisture measurements 142

### 2.2.1. Description of the SSM measurement approach 143

144 At the Agoufou site, soil moisture measurements have been  
 145 specifically designed for remote sensing applications and  
 146 retrieval method validation, therefore a local soil moisture  
 147 station has been installed. It covers a very fine vertical resolution  
 148 in the soil, including SSM measurements at a 5 cm depth. Up-  
 149 scaling features of the SSM, which are of critical importance for  
 150 remote sensing, are addressed through specific SSM measure-  
 151 ment campaigns at a 1 km spatial scale, as described herein.

152 The local station has been continuously measuring soil  
 153 moisture and temperature profiles at a 15-min time interval  
 154 since July, 2004. For soil moisture, a set of five water content  
 155 reflectometers Campbell Scientific CS616 (Campbell Scientific,  
 156 2002) have been installed at 5, 10, 40, 120, 220 cm depths in  
 157 the soil. Gravimetric measurements are performed for calibration  
 158 of the soil moisture sensors at the local scale. The Surface  
 159 Soil Moisture (SSM) is expressed in  $\text{m}^3/\text{m}^3$  (volumetric soil  
 160 water content).

161 In addition to the station measurements, field campaigns  
 162 were conducted in order to estimate SSM at a kilometeric spatial



Fig. 2. View of the Agoufou site.

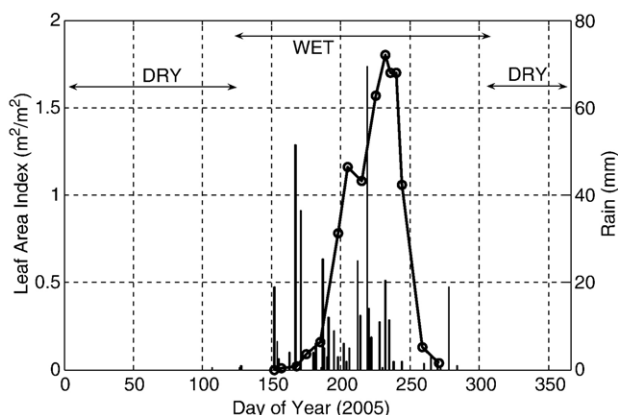


Fig. 3. Temporal evolution of the Leaf Area Index (LAI) and rainfall distribution during the 2005 wet season.

163 scale. For this purpose, a 1 km transect was defined in the E–W  
 164 direction relative to the automatic soil moisture station.  
 165 Measurements are performed with a portable impedance sensor  
 166 every 10 m along this transect, resulting in 100 measurements  
 167 representative of the first 5 cm in the soil (Gaskin & Miller,  
 168 1996). The manufacturer calibration function for sandy soils is  
 169 used to derive volumetric soil moisture values, in agreement  
 170 with a gravimetric calibration performed at different locations  
 171 along the transect. The mean and standard deviation (S.D.) of  
 172 the 100 measurements are computed, and are assumed to be  
 173 representative at the 1 km<sup>2</sup> scale. Field campaigns were con-  
 174 ducted during the 2005 rainy season, providing a total of 25  
 175 SSM measurements for various conditions of surface soil  
 176 moisture.

### 177 2.3. Up scaling local SSM to the kilometric scale

178 Kilometric SSM measurements are shown in Fig. 4 for Day of  
 179 Year (DoY) 223, 225 and 227 (August 2005), following a  
 180 7.5 mm precipitation event on DoY 223 (August 11). For each  
 181 day, the mean value and its standard deviation are represented by  
 182 horizontal and dashed lines, respectively. The SSM measured on  
 183 DoY 223 depicts wet conditions with values of 10.01% with a  
 184 1.28% S.D. The SSM dynamic is shown to be very pronounced  
 185 with a rapid decrease of the mean SSM and standard deviation on  
 186 DoY 225 (mean 5.38%, S.D. 0.99%) and 227 (mean 1.9%, S.D.  
 187 0.79%). Overall, decreases of about 2.5% per day for the 2 first  
 188 days (DoY 223–225), and 1.5% per day for the 2 following days  
 189 are observed. Consequently, the top soil dries out (SSM < 2%)  
 190 within the 5 days following a rainfall event. The relationship  
 191 between the standard deviation and mean SSM has been studied  
 192 for the Agoufou site. Results show that the standard deviation  
 193 increases with the mean of the SSM with a correlation of  
 194  $r=0.85$ . For low values of SSM (1.5%), the standard deviation is  
 195 0.8% and 2% for the highest SSM (16%). This spatial variability  
 196 results from the redistribution of the water at the soil surface due  
 197 to vegetation cover and topography.

198 In this study, transect measurements are used to estimate the  
 199 relationship between SSM at the 1 km scale and the local station  
 200 measurements (Fig. 5). The surface soil moisture at the 1 km

scale is expressed as a function of the local station measure-  
 ments as:

$$\theta_{1 \text{ km}} = 3.945 \times \theta_{\text{Local}} - 65.51 \quad (1)$$

203 where ( $\text{m}^3/\text{m}^3$ ) is the volumetric SSM at the 1 km scale and is  
 204 the local-scale measurement (expressed here in milliseconds).  
 205 Local scale measurements are kept in milliseconds in order to  
 206 avoid potential calibration sensor errors.  
 207

208 The high correlation obtained ( $r=0.97$ ) clearly indicates that  
 209 the dynamic of the SSM at the 1 km scale is strongly correlated  
 210 with the local SSM for a large range of soil moisture conditions  
 211 ranging between 2% and 16%. Accordingly, this transfer  
 212 function is assumed to be suitable to estimate the SSM at a 1 km  
 213 scale from continuous station measurements. In the following,  
 214 this relation is used to compute kilometric SSM values that are  
 215 compared to ASAR data.

### 216 2.4. ENVISAT ASAR data description

217 The ENVISAT satellite was launched by ESA (European  
 218 Space Agency) on March 1, 2002. The ASAR (Advanced  
 219 Synthetic Aperture Radar) instrument is a multi-mode sensor  
 220 which operates at C-band (5.3 GHz) at several polarizations  
 221 (HH, VV, HV and VH), incidence angles, and spatial/  
 222 radiometric resolutions depending on the functioning mode  
 223 (Desnos et al., 1999). At this frequency, atmospheric perturba-  
 224 tions can be considered negligible (Ulaby et al., 1981). The  
 225 satellite passes the descending node at 10:00 a.m. local solar  
 226 time and the ascending node at 22:00 p.m. with a repeat cycle of  
 227 35 days (Louet, 2001). The ASAR instrument may operate as a  
 228 conventional stripmap SAR (Image and Wave modes) or as a  
 229 ScanSAR (Global Monitoring, Wide Swath and Alternating  
 230 Polarization modes) (Torres et al., 1999; Zink, 2002). A more  
 231 detailed description of the ASAR specifications can be found in  
 232 Baup et al. (2006).

233 In the present study, emphasis is placed on the Wide Swath  
 234 (WS) mode at HH polarization. For this mode, the spatial  
 235 resolution is 150 m and the incidence angles range between 16°  
 236 and 43° (ENVISAT handbook, 2004). For the considered period,

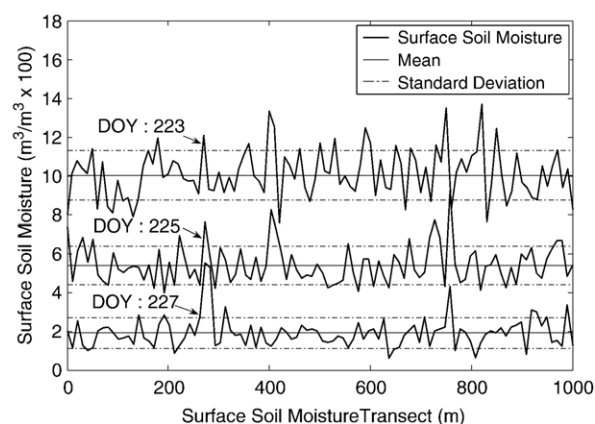


Fig. 4. Temporal Surface Soil Moisture measurements along the 1 km transect (DoY: 223, 225 and 227 of 2005) following a rainfall event on DoY 223.

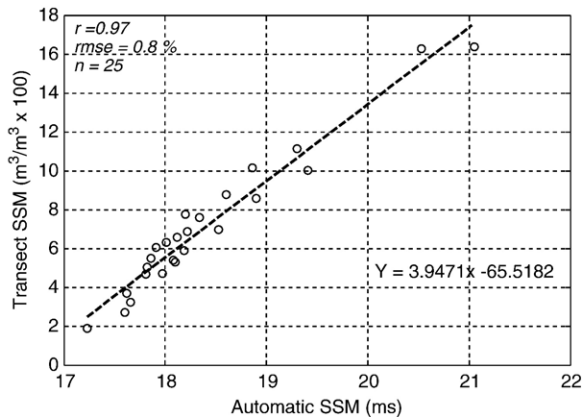


Fig. 5. Comparison between Surface Soil Moisture measurements along the 1 km transect (in %) and data collected by the automatic soil moisture station in milliseconds (July–August 2005).

237 from July to December, 2005, the number of available data over  
 238 the Agoufou site is about 2–3 images/decade (i.e. a 10-day  
 239 period), allowing the monitoring of short scale land processes  
 240 such as the soil moisture variation. However, these images are  
 241 acquired at different incidence angles compared to those  
 242 recorded at a 35-day interval. No azimuthal difference linked  
 243 to the acquisitions made during ascending or descending passes  
 244 has been observed for the Agoufou site. Accordingly, in the  
 245 following, data from the two different orbits are mixed together.  
 246 The calibration process is performed using the B.E.S.T (Basic  
 247 ENVISAT SAR Toolbox) software provided by ESA. Details on  
 248 the calibration algorithm can be found in Laur et al. (1998). The  
 249 geocoding is performed using the IDL/ENVI software and the  
 250 results are assessed by superimposing an ASAR image onto a  
 251 Landsat TM (30 m resolution). For a  $1 \times 1$  km<sup>2</sup> window, the  
 252 estimated confidence interval for the backscattering coefficient  $\sigma^0$   
 253 after angular normalization is  $\pm 0.65$  dB (at  $1\sigma$ ) (Baup et al., 2006).

#### 254 2.5. Methodology

255 Three different approaches for SSM retrieval from ASAR  
 256 data are investigated in this study. The proposed approaches  
 257 differ from the normalization procedure that is used to correct  
 258 the angular variations of the radar signal. For the 3 considered  
 259 methods, soil roughness in terms of height root mean square  
 260 (hrms) and correlation length is assumed to be constant over the  
 261 studied period (Jarlan et al., 2002; Wagner & Scipal, 2000). The  
 262 particularity of the studied area is the low observed SSM values  
 263 which range between 0.5% and 12% for the whole period under  
 264 consideration. All ASAR and SSM data used are summarized in  
 265 Table 1.

266 In the first approach, hereafter referred to as [N23], the whole  
 267 ASAR data set is considered for the comparison with the SSM  
 268 values. The number of available data is about 2–3 samples per  
 269 decade. The approach consists of using all data acquired at  
 270 various incidence angles during the dry period to establish the  
 271 angular regression function which is approximated by a second  
 272 order polynomial fit. Then, this function is used to normalize the  
 273 entire data set at an incidence angle of  $23^\circ$  assuming that there is

no variation of the fit during the year. This is a reasonable  
 274 assumption since the chosen incidence angle ( $23^\circ$ ) is located  
 275 where the effects of vegetation are minimized. In addition, the  
 276 normalization errors that result from the effects of vegetation at  
 277 high incidence angles ( $>30^\circ$ ) are expected to be small due to the  
 278 low vegetation density and are thus neglected (Ulaby et al.,  
 279 1982). Moreover, at a  $23^\circ$  incidence angle the influence of the  
 280 soil roughness is also minimized (Ulaby & Bativala, 1976;  
 281 Ulaby et al., 1978; Sano et al., 1997).  
 282

The second method, [N23\_season], takes into account the  
 283 seasonal vegetation effect on the angular variation of the  
 284 backscattered coefficient. In this case, two normalization  
 285 functions depending on the season are used. For the dry season  
 286 (from January to May and from October to December), which is  
 287

Table 1

Date, incidence angle, backscattering coefficient and kilometric surface soil moisture values before angular normalization of the Wide Swath ASAR data (HH polarization)

Month	Day	Time	Incidence angle ( $^\circ$ )	Backscattering coefficient ( $\text{m}^2/\text{m}^2$ )	Kilometric surface soil moisture ( $\text{m}^3/\text{m}^3 * 100$ )
07	16	10:03:41	23.65	0.0607	5.72
07	29	09:55:09	38.04	0.0238	1.83
08	01	10:00:48	28.86	0.0618	8.56
08	05	22:17:36	39.96	0.0396	3.09
08	14	09:52:16	42.09	0.0356	3.70
08	17	09:57:56	33.65	0.0569	8.88
08	20	10:03:36	23.70	0.966	11.92
09	2	09:55:05	38.02	0.0335	6.25
09	3	22:06:13	20.83	0.0496	2.56
09	5	10:00:45	28.84	0.0282	1.87
09	6	22:11:53	31.17	0.0282	1.47
09	8	10:06:25	18.13	0.0396	1.52
09	9	22:17:34	40.03	0.0215	1.29
09	18	09:52:15	42.04	0.0204	1.14
09	21	09:57:56	33.63	0.0178	1.03
09	22	22:09:04	26.21	0.0583	3.98
09	24	10:03:36	23.68	0.0403	1.56
09	25	22:14:45	35.79	0.0232	1.03
10	7	09:54:56	38.06	0.0255	6.77
10	8	22:06:25	20.82	0.0581	3.94
10	10	10:00:36	28.86	0.0268	2.89
10	13	10:06:16	18.17	0.0623	1.69
10	14	22:17:46	40.00	0.0215	1.38
10	23	09:52:06	42.05	0.0176	1.07
10	26	09:57:47	33.61	0.0212	0.85
10	27	22:09:17	26.22	0.0327	0.76
10	29	10:03:27	23.66	0.0435	0.81
11	11	09:54:56	38.02	0.0145	0.61
11	12	22:06:25	20.85	0.0487	0.58
11	15	22:12:05	31.17	0.0194	0.56
11	17	10:06:15	18.14	0.0541	0.65
11	18	22:17:45	39.98	0.0127	0.54
11	27	09:52:02	42.07	0.0124	0.67
11	30	09:57:42	33.68	0.0163	0.65
12	1	22:09:11	26.12	0.0261	0.60
12	4	22:14:51	35.72	0.0188	0.50
12	16	09:54:50	38.06	0.0138	0.52
12	17	22:06:19	20.79	0.0458	0.41
12	19	10:00:29	28.87	0.0218	0.54
12	20	22:11:58	31.13	0.0191	0.43
12	22	10:06:09	18.16	0.0560	0.52
12	23	22:17:38	39.96	0.0120	0.47

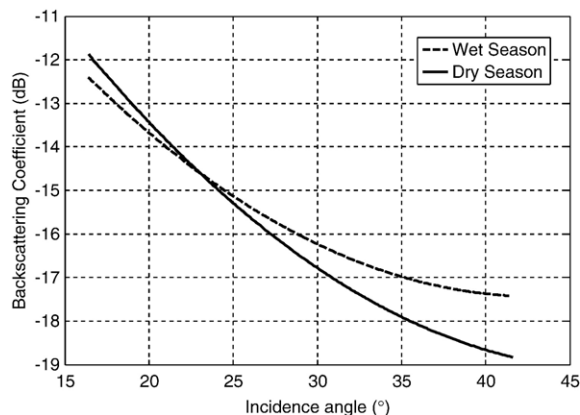


Fig. 6. Angular variations of the HH backscattering coefficient during the dry and wet seasons for the sand dune landscape estimated for the 2005 dry period and on DoY 248.

288 when the green vegetation cover is small or absent, the  
 289 normalization function reverts to the previously established  
 290 relationship [N23]. For the wet season, a simple normalization  
 291 function is built by considering all of the ASAR data recorded at  
 292 the date of maximum green vegetation cover. Fig. 6 illustrates  
 293 the angular dependency of the radar signal during the dry (no  
 294 vegetation) and the wet seasons (maximum of vegetation). The  
 295 wet regression is estimated from a radar image acquired in  
 296 September (DoY 248), when soil surface is getting drier and  
 297 green vegetation is closed to its maximum (DoY 232). The  
 298 resulting angular functions show that the effect of the vegetation  
 299 layer has to be taken into account in the normalization  
 300 procedure. Here, this is simply done by considering a sole  
 301 ‘average’ normalization function for the whole rainy period,  
 302 whatever the vegetation cover is. In contrast to previous studies  
 303 (Le Hegarat-Masclé et al., 2002; Wang et al., 2004), this method  
 304 does not require the use of ancillary data. The seasonal  
 305 vegetation effect is simply taken into account from the seasonal  
 306 analysis of the ASAR data. As for method [N23], the number of  
 307 available data is about 2–3 samples per decade.

308 The third method [N23\_season\_lowangle], also considers  
 309 two different regression functions depending on the season, but  
 310 the data under consideration are restricted to those acquired at  
 311 an incidence angle lower than  $30^\circ$  in order to minimize soil  
 312 roughness and vegetation effects. In this case, the number of  
 313 available data is about 1.2 samples per decade. At a  $23^\circ$   
 314 incidence angle, model simulations (Baup et al., 2006) based on  
 315 the approach proposed by Karam et al. (1992), Frison et al.  
 316 (1998) and Jarlan et al. (2002), indicate that the measured  
 317 backscatter originates from two main contributions, namely the  
 318 soil surface and the interaction between the soil and the  
 319 vegetation. These contributions are mainly driven by SSM  
 320 which controls the dielectric properties of the upper soil profile.

### 321 3. Surface soil moisture estimation

322 Relationships between SSM kilometric measurements and  
 323 normalized  $\sigma^0$  estimated within a  $1 \times 1 \text{ km}^2$  window are examined  
 324 in this section. The study is mainly performed for the Agoufou

325 site. The robustness of the observed relationships is measured  
 326 using a correlation and root mean square error (rmse) analysis.  
 327 Finally, the best inversion method is used to derive time series of  
 328 SSM that are compared to the automatic kilometric-scale SSM.

#### 329 3.1. Relationships between SSM and normalized $\sigma^0$

330 Fig. 7(a–c) illustrate the comparison between kilometric  
 331 SSM and the normalized backscattering coefficients derived

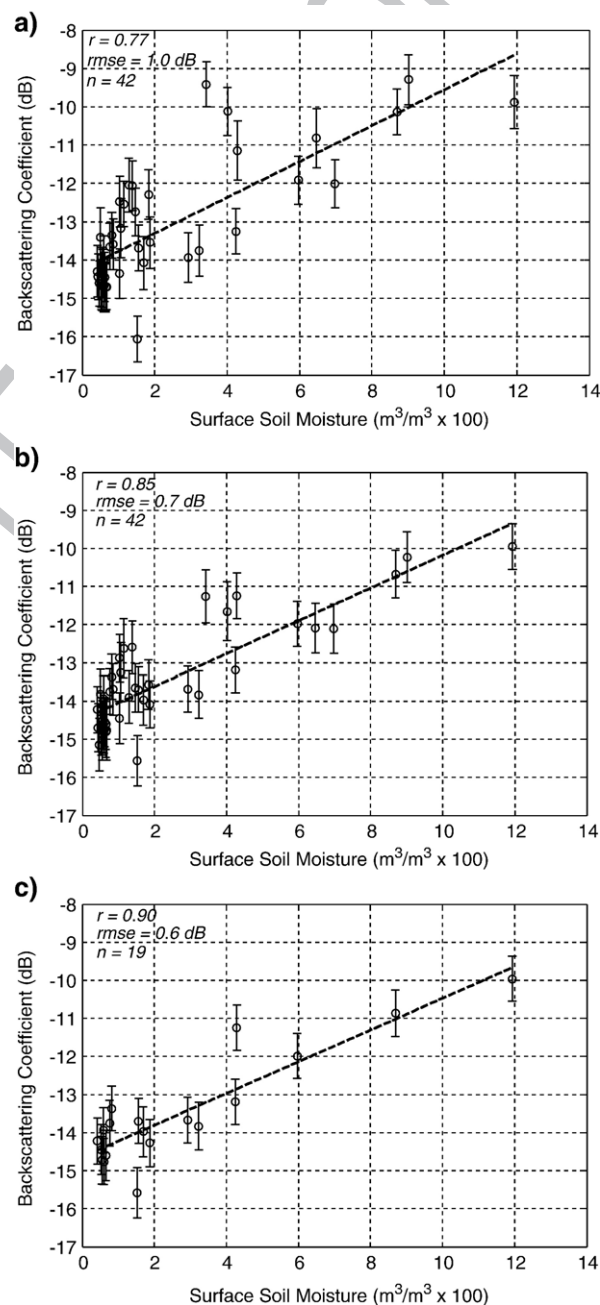


Fig. 7. a) Normalized HH backscattering coefficient versus Surface Soil Moisture for WS mode at HH Polarization (2005 rainy season). b) Normalized HH backscattering coefficient using two different functions (dry and wet season) versus the Surface Soil Moisture content for WS mode at HH Polarization. c) Normalized HH backscattering coefficient, estimated at low incidence angle ( $<30^\circ$ ), versus the Surface Soil Moisture content for WS mode at HH Polarization.

332 from the [N23], [N23\_season] and [N23\_season-lowangle]  
 333 methods, respectively. For the 3 methods under consideration,  
 334 results show a significant linear correlation between SSM and  
 335 the normalized  $\sigma^0$ , the best performance being obtained with  
 336 the [N23\_season-lowangle] method. Calculated correlation  
 337 coefficients,  $r$  (and associated rmse in dB) are 0.77 (1.0), 0.85  
 338 (0.7), 0.90 (0.6) for the [N23], [N23\_season] and [N23\_season-  
 339 lowangle] methods, respectively (Table 2). Whatever the  
 340 method used, a large scatter in  $\sigma^0$  appears especially at low  
 341 SSM. Although it is related to the large amount of radar data  
 342 recorded during the dry season, this large scatter is not in  
 343 agreement with the observed features of SSM spatial variability  
 344 (Fig. 4). Since the scatter is mainly observed during the dry  
 345 season, it is assumed to be mostly related to satellite  
 346 measurement noise and possible small surface roughness  
 347 variations. Moreover, it is of importance to notice that the  
 348 scatter of  $\sigma^0$  data ranges within its normal error range (at  $1\sigma$ ).

### 349 3.2. Effect of seasonal vegetation dynamics on SSM estimation

350 For both [N23\_season] and [N23\_season\_lowangle] meth-  
 351 ods, effects of vegetation on surface backscattering coefficient  
 352 are taken into account by simply using a wet and a dry season  
 353 normalization function, as depicted in Fig. 6. This method does  
 354 not require any ancillary information on the vegetation status.  
 355 To further investigate the effect of vegetation on soil moisture  
 356 retrieval performance, seasonal features of the angular varia-  
 357 tions of the backscattering coefficient are addressed in this  
 358 subsection through the use of ancillary LAI information. For  
 359 each day, a sigma normalization function is interpolated  
 360 between the dry and wet curves, based on a linear weighting  
 361 function of the observed LAI. The corresponding date  
 362 normalization function is then applied for the N23\_season  
 363 method, for which the whole ASAR data set is used whatever  
 364 the incidence angle is. Results using this method ( $r=0.83$ ,  
 365  $\text{rmse}=1.5\%$ ) are similar to those obtained without LAI  
 366 information ( $r=0.85$ ,  $\text{rmse}=1.4\%$ ).

367 The absence of improvement is mainly related to the low  
 368 vegetation density. Accordingly, no ancillary information on  
 369 LAI is used in the following.

### 370 3.3. Inverted time series of SSM

371 Results obtained with the [N23\_season-lowangle] are  
 372 presented for the July–December period, using the statistical  
 373 relationship linking  $\sigma^0$  and SSM, and by assuming that the  
 374 minimum SSM value is 0.5%. These estimates are compared to

t2.1 Table 2  
 Comparison of the three methods in terms of correlation coefficient, rms errors  
 t2.2 (in % and in dB) and final SSM estimations errors

t2.3		$r$	$\sigma^0$ rmse	SSM rmse	Final SSM error (with radar errors (2.4%) and up-scaling SSM function (0.8%))
t2.4	N23	0.77	1.0 dB	1.7%	3.0%
t2.5	N23_season	0.85	0.7 dB	1.4%	2.9%
t2.6	N23_season_lowangle	0.90	0.6 dB	1.3%	2.8%

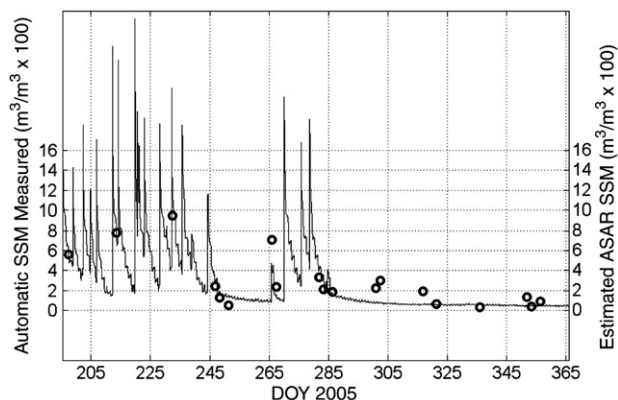


Fig. 8. Temporal variation of automatic SSM measurements and satellite-derived SSM using ASAR data acquired at low incidence angles ( $<30^\circ$ ) for the Agoufou site (July–December 2005).

the kilometric-scale SSM measurements derived from the  
 automatic local-scale measurements recorded at the satellite-  
 overpass time. Results show a very good agreement between  
 ASAR-derived SSM and SSM measurements (Fig. 8). The  
 associated correlation coefficient is  $r=0.90$  with a  $\text{rmse}=1.3\%$   
 ( $n=19$ ). Compared to the two other methods, the improvement  
 is 30% and 40% in terms of rms errors of the backscattering  
 coefficient with values of 1.0 dB, 0.7 dB and 0.6 dB for the  
 N23, N23\_season and N23\_season\_lowangle methods, respec-  
 tively (Table 2). Similar improvement is observed when  
 considering the rms error on the SSM from the model inversion.  
 However, the main drawback of this method is the reduction by  
 a factor of two of the temporal sampling.

A suitable estimate of measure errors must also take into  
 account two other error sources:

- the confidence interval of the backscattering coefficient  
 ( $\pm 0.6$  dB) and the angular normalization error (mean equal to  
 0.25 dB), implying a mean radar processing error of 0.65 dB  
 and a SSM error of 2.4%;
- the rms error due to the kilometric transfer function (0.8%).

Consequently, the resulting accuracy of the inverted SSM is  
 3.0%, 2.9% and 2.8% for the 3 methods, respectively, with the  
 most significant error contribution being due to the radar  
 accuracy (2.4%).

## 4. Concluding remarks

Relationships between Surface Soil Moisture, SSM, of  
 Sahelian sandy soil and the ASAR backscattering coefficient at  
 HH polarization are examined in this study. First, a transfer  
 function is established for up-scaling local SSM measurements  
 to the 1 km scale which is compatible with the ASAR estimated  
 backscattering coefficients. Second, three radar signal angular  
 normalization methods are tested. The proposed approaches  
 differ in terms of the inclusion of vegetation effects in the  
 correction. In addition, the third method is restricted to radar  
 data which are acquired at low incidence angles in order to  
 minimize the influence of vegetation and soil roughness.

Results show a strong linear relationship between SSM and HH normalized backscattering coefficients indicating the high capabilities of the ASAR instrument to estimate SSM in a semiarid environment even at very low SSM (ranged between 0.5% and 12%). Whereas studies based on SSM estimation using SAR data in semiarid rangelands generally deal with an increased range of SSM values (up to 30% larger) and do not indicate a significant relationship for low SSM ( $<15^\circ$ ) (Mattia et al., 2006; Moran et al., 2000). Results also clearly demonstrate that the vegetation effects have to be taken into account in order to improve the angular normalization procedure. These effects can be corrected using only multi-angular ASAR data, and the use of LAI data is not necessary for low LAI $<2.0$ . Although the vegetation effects are not perfectly known, especially at high incidence angles, the N23\_method presented in this paper gives preliminary quantitative results, and the rms error of the Surface Soil Moisture retrieval is 2.9%. By considering only the data acquired at an incidence angle lower than  $30^\circ$ , the rms error is slightly reduced to 2.8%. This small improvement is obtained because the main error source comes from the  $\sigma^0$  confidence interval (2.4%). Moreover, the last method reduces temporal repetitivity (1.2 data samples per decade compared to 2.8) and it would be of interest to retain the highest temporal sampling of SSM while keeping a good accuracy of the SSM retrieval. This is especially important for the Sahel, where the top surface of sandy soils dries quickly after rainfall events.

## 5. Uncited reference

ENVISAT ASAR product handbook, 2004

## Acknowledgements

This work was performed within the framework of the AMMA project. Based on a French initiative, AMMA has been constructed by an international group and is currently funded by large number of agencies, especially from France, the UK, the US and Africa. It has been the beneficiary of a major financial contribution from the European Community's Sixth Framework Research Programme. Detailed information on the scientific coordination and funding is available on the AMMA international web site (<https://www.amma-eu.org/>). The authors thank ESA for providing the ENVISAT data used in the present study (Project ID 443, E. Mougin). The authors are grateful for all the help they received during the field measurement campaigns, especially from their colleagues and collaborators from the national institute for agronomic research in Mali, the 'Institut d'Economie Rurale'. The authors also thank Aaron Boone whose suggestions helped improve an earlier draft.

## References

Baup, F., Mougin, E., Hiernaux, P., Lopes, A., De Rosnay, P., & Ch enerie, I. (2006). Radar signatures of Sahelian surfaces in Mali using ENVISAT-ASAR data. *IEEE Transactions on Geoscience and Remote Sensing* (in revision).  
Campbell Scientific. (2002). *CS616 Water Content Reflectometer*. User guide, Issued 6.3.02.

Chanzy, A., Schmugge, T. J., Calvet, J. -C., Kerr, Y., Oevelen, P. V., Grosjean, O., et al. (1997). Airbone microwave radiometry on a semiarid area during HAPEX-Sahel. *Journal of Hydrology*, 188–189, 285–309.  
Clark, D. B., Taylor, C. M., & Thorpe, A. J. (2004). Feedback between the land surface and rainfall at convective length scales. *Journal of Hydrometeorology*, 5, 625–639.  
Desnos, Y. L., Laur, H., Lim, P., Meisl, P., & Gach, T. (1999). The ENVISAT-1 advanced synthetic aperture radar processor and data products. *Geoscience and Remote Sensing Symposium, IGARSS'99, Hamburg, Germany* (pp. 1683–1685).  
Engman, E. T. (1990). Progress in microwave remote sensing of soil moisture. *Canadian Journal of Remote Sensing*, 16(3), 6–14.  
ENVISAT ASAR product handbook. (2004). *European Space Agency*. Issue 1.2.  
Frison, P. L., Mougin, E., & Hiernaux, P. (1998). Observations and interpretation of seasonal ERS-1 wind scatterometer data over Northern Sahel (Mali). *Remote Sensing of Environment*, 63, 233–242.  
Gaskin, G. J., & Miller, J. D. (1996). Measurement of soil water content using a simplified impedance measuring technique. *Journal of Agricultural Engineering Resources*, 63, 153–160.  
GEWEX-news. (2006). Global Energy and Water Cycle Experiment, special issue 'AMMA west African monsoon studies are addressing water cycle issues' 16 (1).  
Jarlan, L., Mazzega, P., Mougin, E., Lavenu, F., Marty, G., Frison, P. L., et al. (2003). Mapping of Sahelian vegetation parameters from ERS scatterometer data with an evolution strategies algorithm. *Remote Sensing of Environment*, 87, 72–84.  
Jarlan, L., Mougin, E., Frison, P. L., Mazzega, P., & Hiernaux, P. (2002). Analysis of ERS wind scatterometer time series over Sahel (Mali). *Remote Sensing of Environment*, 81, 404–415.  
Karam, M. A., Fung, A. K., Lang, R. H., & Chauhan, N. S. (1992). A microwave scattering model for layered vegetation. *IEEE Transactions on Geoscience and Remote Sensing*, 30, 767–784.  
Koster, R. D., Dirmeyer, P. A., Guo, Z., Bonan, G., Chan, E., Cox, P., et al. (2004). Regions of strong coupling between soil moisture and precipitation. *Sciences*, 305, 1038–1040.  
Laur, H., Bally, P., Meadows, P., Sanchez, J., Schattler, B., Lopinto, E., et al. (1998). *Derivation of the backscattering coefficient so in ESA SAR products*. ESA publication, Document No: ES-TN-RS-PM-HL09 17, Issue 2, Rev. 5d.  
Le Hegarat-Mascl e, S., Zribi, M., Alem, F., Weisse, A., & Loumagne, C. (2002). Soil moisture estimation from ERS/SAR data: Toward an operational methodology. *Transactions on Geoscience and Remote Sensing*, 40, 2647–2658.  
Louet J. (2001). The Envisat Mission and System. In b. 106 (Ed.). Available: [http://www.esa.int/esapub/bulletin/bullet106/bul106\\_1.pdf](http://www.esa.int/esapub/bulletin/bullet106/bul106_1.pdf)  
Magagi, R. D., & Kerr, Y. H. (1997). Retrieval of soil moisture and vegetation characteristics by use of ERS-1 wind scatterometer over arid and semiarid areas. *Journal of Hydrology*, 188–189, 361–384.  
Mattia, F., Satalino, G., Dente, L., & Pasquariello, G. (2006). Using a priori information to improve soil moisture retrieval from ENVISAT ASAR AP data in semiarid regions. *IEEE Transactions on Geoscience and Remote Sensing*, 44, 900–912.  
Monteny, B. A., Lhomme, J. P., Chehbouni, A., Troufleau, D., Amadou, M., Sicot, M., et al. (1997). The role of the Sahelian biosphere on the water and the CO<sub>2</sub> cycle during the HAPEX-Sahel experiment. *Journal of Hydrology*, 188–189, 516–535.  
Moran, M. S., Hymer, D. C., Qi, J., & Sano, E. E. (2000). Soil moisture evaluation using-temporal synthetic aperture radar (SAR) in semiarid rangeland. *Agricultural and Forest Meteorology*, 105, 69–80.  
Njoku, E., Jackson, T., Lakshmi, V., Chan, T., & Nghiem, S. V. (2003). Soil moisture retrieval from AMSR-E. *IEEE Transactions on Geoscience and Remote Sensing*, 41(2), 215–229.  
Sano, E. E., Moran, M. S., Huete, A. R., & Miura, T. (1997). C- and multiangle Ku-band synthetic aperture radar data for bare soil moisture estimation in agricultural areas. *Remote Sensing Environment*, 64, 77–90.  
Satalino, G., Mattia, F., Davidson, M. W. J., Toan, T. L., Pasquariello, G., & Borgeaud, M. (2002). On current limits of soil moisture retrieval from ERS-SAR data. *Transactions on Geoscience and Remote Sensing*, 40, 2438–2447.  
Schmugge, T., Jackson, T., Kustas, T. J., & Wang, J. R. (1992). Passive microwave remote sensing of soil moisture: Results from HAPEX, FIFE and MONSOON'90. *ISPRS Journal of Photogrammetry and Remote Sensing*, 47, 127–143.

- 531 Stephen, H., & Long, D. G. (2004). Analysis of scatterometer observations of  
532 Saharian ergs using a simple rough facet model. *IEEE Transactions on*  
533 *Geoscience and Remote Sensing, Geoscience and Remote Sensing*  
534 *Symposium, IGARSS'04, Proceedings, vol. 3* (pp. 1534–1537).
- 535 Tansey, K. J., Millington, A. C., Battikhi, A. M., & White, K. H. (1999).  
536 Monitoring soil moisture dynamics using satellite imaging radar in  
537 northeastern Jordan. *Applied Geography, 19*, 325–344.
- 538 Taylor, C. M., & Ellis, R. J. (2006). Satellite detection of soil moisture impacts  
539 on convection at the mesoscale. *Geophysical Research Letters, 33*.  
540 doi:10.1029/2005GL02525
- 541 Taylor, C. M., Parker, D. J., Lloyd, C. R., & Thorncroft, C. D. (2005).  
542 Observations of synoptic scale land surface variability and its coupling with  
543 the atmosphere. *Quarterly Journal of the Royal Meteorological Society, 13*,  
544 913–938.
- 545 Torres, R., Buck, C., Guijarro, J., Suchail, J. L., & Schöenberg, A. (1999). The  
546 ENVISAT ASAR instrument verification and characterisation. *CEOS SAR*  
547 *Workshop. Toulouse, France.*
- 548 Ulaby, F. T. (1975). Radar Response to vegetation. *IEEE Transaction on*  
549 *Antennas and Propagation, AP-23*, 36–45.
- 550 Ulaby, F. T., & Batlivala, P. P. (1976). Optimum radar parameters for mapping  
551 soil moisture. *IEEE Transaction on Geoscience Electronics, 14*(2), 81–93.
- 552 Ulaby, F. T., Batlivala, P. P., & Dobson, M. C. (1978). Microwave backscatter  
553 dependence on surface roughness, soil moisture and soil texture: Part I—  
554 Bare soil. *IEEE Transactions on Geoscience Electronics, 16*(4), 286–295.  
579
- Ulaby, F. T., Fung, A. K., & Moore, R. K. (1981). *Microwave and remote*  
555 *sensing active and passive*. Norwood, MA: Artech House. 556
- Ulaby, F. T., Fung, A. K., & Moore, R. K. (1982). *Microwave and remote*  
557 *sensing: Active and passive: Surface scattering and emission theory*. 558
- Ulaby, F. T., Fung, A. K., & Moore, R. K. (1986). *Microwave and remote*  
559 *sensing active and passive*. Norwood, MA: Artech House. 560
- Wagner, W., & Scipal, K. (2000). Large-scale Soil moisture mapping in western  
561 Africa using the ERS scatterometer. *IEEE Transactions on Geoscience and*  
562 *Remote Sensing, 38*, 1777–1782. 563
- Wang, C., Qi, J., Moran, S., & Marsett, R. (2004). Soil moisture estimation in a  
564 semiarid rangeland using ERS-2 and TM imagery. *Remote Sensing of*  
565 *Environment, 90*, 178–189. 566
- Weiss, M., Baret, F., Smith, G. J., Jonckheere, I., & Coppin, P. (2004). Review of  
567 methods for in situ leaf area index (LAI) determination. Part II. Estimation of  
568 LAI, errors and sampling. *Agricultural and Forest Meteorology, 121*, 37–53. 569
- Woodhouse, I. H., & Hoekman, D. H. (2000). Determining land surface  
570 parameters from the ERS-1 wind scatterometer. *IEEE Transactions on*  
571 *Geoscience and Remote Sensing, 38*, 126–140. 572
- Zink, M. (2002). Introduction to the ASAR calibration/validation project. *The*  
573 *Envisat calibration review. Noordwijk (The Netherlands)*. 574
- Zribi, M., Le Hegarat-Masclé, S., Otle, C., Kammoun, B., & Guerin, C. (2003).  
575 Surface soil moisture estimation from the synergistic use of the (multi-incidence  
576 and multi-resolution) active microwave ERS wind scatterometer and SAR data.  
577 *Remote Sensing of Environment, 86*, 30–41. 578